



# INTERACTION OF A SHEAR LAYER WITH A FREE SURFACE

Dana Dabiri<sup>1</sup> & Mory Gharib<sup>2</sup>

**Keywords:** *Shear layer, turbulence, free surface, DPIV*

## ABSTRACT

A newly developed non-intrusive method has been developed for studying near surface flows, allowing for measurements of both small-sloped free surface deformations as well as near surface velocities. This technique combines Digital Particle Image Velocimetry (DPIV) and the reflective mode of the free surface gradient detector (FSGD) technique into a single measurement system. Using this system, correlations between elevation and kinematic properties, such as velocity and vorticity, which is important in understanding near surface turbulence, are obtained. This system is explained and demonstrated by measuring these correlations for a vertical shear layer intersecting a free surface.

## 1 INTRODUCTION

Free surface flows are phenomena that are subject to great interest since they are abundantly evident in both nature and flows of practical importance. For example, from an environmental point of view, free surface flow phenomena, such as wave breaking, are responsible for heavy air, and therefore oxygen, entrainment into the oceans, while the fluid turbulence allows for distribution of the entrained oxygen to allow for the existence of life within the oceans. Furthermore, from a practical point of view, flow about surface moving vehicles typically result in persistent wakes that last over several hundred kilometers, thereby raising concerns regarding not only drag, but also stealth. To fully understand these flows, it is therefore necessary to understand the interaction between the near surface turbulence with the free surface, the resulting deformation of the free surface, and finally the resulting turbulence near the surface do to this interaction for a variety of Froude numbers.

For low Froude numbers, Dommermuth et al. [1] shows that the equations of motions could be reduced to:

$$\begin{aligned}\frac{\partial U_i^r}{\partial \tilde{t}} + U_j^r \frac{\partial U_i^r}{\partial x_k} &= -\frac{\partial P^r}{\partial \tilde{x}_i} + \frac{1}{\text{Re}} \frac{\partial^2 U_i^r}{\partial x_j^2} + \mathbf{a}f(U_i^r), \\ \frac{\partial U_i^r}{\partial \tilde{x}_i} &= 0; \quad \frac{\partial^2 P^r}{\partial x_j^2} = -\frac{\partial U_j^r}{\partial \tilde{x}_i} \frac{\partial U_i^r}{\partial \tilde{x}_j} \text{ for } \tilde{z} \leq 0; \\ W^r &= 0 \text{ and } \frac{1}{Fr^2} \mathbf{h}^r = -P_a + P^r \text{ for } \tilde{z} = 0\end{aligned}$$

where the superscript  $r$  refers to components that contribute to the free surface roughness,  $\mathbf{h}$  is the free surface elevation,  $P$  is the pressure normalized by the density,  $U$  is the velocity, the subscript  $a$  refers to atmospheric conditions,  $\mathbf{a}$  is a source coefficient and  $f$  is a linear operator. Specifically, the last equation shows that in the absence of atmospheric pressure, the surface elevation is

**Author(s):** <sup>1</sup>301-46 Caltech, Pasadena CA 91125.  
<sup>2</sup>205-45 Caltech, Pasadena CA 91125.

*Corresponding Author: Dana Dabiri*

hydrostatically balanced by the vortically induced pressure. This, therefore allows the measurement of pressure near the surface through the measurement of the free surface elevation. Beuther et al. [2] and George et al. [3], showed that for a homogeneous constant mean shear flow, the pressure spectra is composed of a 2<sup>nd</sup> moment turbulence-mean-shear interaction with a  $-11/3$  slope, a turbulence-turbulence interaction with a  $-7/3$  slope, and lastly a 3<sup>rd</sup> moment turbulent-mean-shear interaction term with a  $-3$  slope. It is thus one of the goals of this paper to measure the free surface elevation spectra, and therefore the surface pressure, in order to confirm the results obtained by Beuther et al., and George et al. Lastly, to better our understanding of the interaction of the free surface with the near surface turbulence for low Froude number flows, various correlations are performed between the kinematic flow variables, such as velocity and vorticity, and the free surface deformation, in order to best determine the relevant turbulent flow parameters responsible for the free surface deformation.

Velocity measurements have been dramatically developed through the advent of the DPIV techniques in the last decade. However, free surface measurement methods have not enjoyed such attention. Cox [4] was the first to contribute to these methods by developing a single point, single slope component detector. The first method capable of measuring two-slope component measurements within a two-dimensional domain was developed by Zhang & Cox [5]. By using a discrete color palette, they were able to map a one-to-one correspondence between color and slope. Furthermore, as their slopes were high, they implemented a refractive setup to their free surface gradient detector (FSGD). To obtain more accurate results, Jähne [6] and Balschbach et al. [7] used a continuous, rather than a discrete color palette. While these methods were applied to photographic images, only recently has it been possible to acquire time-evolving images through the advent of video technology. Dabiri et al. [8], Zhang et al. [9] and Dabiri et al. [10] demonstrated the real-time acquisition of the FSGD using the refractive color-coding scheme.

In order to study the near surface turbulence and its interaction with the free surface, a shear layer is generated such that the axis of its main rollers are perpendicular to the free surface. The interaction of the shear layer with the free surface is then studied in order to identify the dominant correlations between the free surface deformation and the kinematic field directly below.

## 2 EXPERIMENTAL SETUP

### 2.1 Free Surface Gradient Detector

#### 2.1.1 Operating Principle

The operating principle behind the FSGD is to establish a one-to-one correspondence between color and slope, thereby color-coding each of the different slopes with different colors (Zhang & Cox [5]; Zhang, et al [8]; Dabiri, et al. [9]). There are two types of setups possible for the FSGD system. The first is the *refractive mode*, which is used for cases where the slope variations are large. The second is the *reflective mode*, which is used for cases where slope variations are small. As the range of free surface slopes for the present setup are small, the reflective mode is used.

The operational diagram of the reflective mode is shown in figure 1. A color palette, when placed in front of a diffused white light source, will illuminate each of the colors in all directions. A lens, placed at a distance of one focal length away from the color palette, will make all of the rays of each color become parallel. However, each of the parallel set of colored beams will be oriented in different directions with respect to other colored light rays. This system of parallel color beams is used to illuminate the free surface. For various free surface deformations, there is only one free surface slope that will reflect a particular color towards an observer located far away. This is how a one-to-one correspondence between color and free surface slopes is achieved.

#### 2.1.2 Color Palette

For a reflective system, the angle of the incident and reflected beams from the free surface are equal. Therefore, the largest angles that can be measured is a function of the diameter of the lens,  $D$ , its focal length,  $f$ , and the diameter of the color palette,  $D_c$ , and is:

$$\mathbf{a}_{\max} = \tan^{-1}\left(\frac{D_s}{2f}\right) \leq \tan^{-1}\left(\frac{D}{2f}\right) = \tan^{-1}\left(\frac{1}{2F\#}\right). \quad (1)$$

where  $\mathbf{a}_{\max}$ , is the largest angle measurable (see figure 2).

Equation 1 also shows that if the size of the palette is equal to the size of the lens, the maximum measurable angle can be determined by the  $F\#$  of the lens. By geometry, the maximum measurable area,  $L_{\max}$  can be shown to be

$$L_{\max} = D \cos \mathbf{b}_0 - \left(H - \frac{D}{2} \sin \mathbf{b}_0\right) \tan \mathbf{b}_{\max} - \left(H + \frac{D}{2} \sin \mathbf{b}_0\right) \tan(\mathbf{b}_{\max} - 2\mathbf{b}_0). \quad (2)$$

where  $D$  is the size of the lens,  $\mathbf{b}_0$  is the angle between the optical axis and the free surface normal,  $H$  is the vertical height of the center of the lens to the free surface, and  $\mathbf{b}_{\max}$  is the largest possible angle between the light rays and the free surface normal (see figure 3).

Previous systems using discrete color palettes had two problems. First, the number of colors limited the number of slopes that could be measured (see figure 3). Second, the intensity variations resulted in poor measurements for the lower intensity colors. Therefore, as proposed by Jähne [5] and Balschbach et al. [7], a continuously varying color map shown in figure 4 is used, where green varies linearly in the x- direction, and red and blue vary linearly in the y- direction. Each of these colors is then recombined and normalized so that

$$3G/(R+G+B) \quad (6)$$

varies linearly in the x-direction, and

$$3(R-B)/(R+G+B) \quad (7)$$

varies linearly in the y-direction. Since this color palette is continuous and normalized by the intensity, it has the advantage of increasing the slope sensitivity as well as compensating for spatial intensity variations.

### 2.1.3 Calibration

In order to convert from the color images to the free surface slopes, it is necessary to create a conversion table. It is important that the calibration be done in the exact same setup as the experiment, as the data acquired is highly dependent on the setup of the FSGD. The calibration is performed by first placing a spherical mirror of known curvature within the desired measurable area. The FSGD illuminates the spherical mirror, and the rays collected by the color camera from the spherical mirror are saved as the color calibration image. Since the slopes of the spherical mirror are known, a lookup table can be easily constructed using the colors and their corresponding slopes.

### 2.1.4 Free Surface Elevation Extraction

The acquired images are slightly noisy due to the low lighting conditions and the camera's electronics. Therefore, the image noise is removed by applying a median filter to all the acquired images. Once this noise is removed, the color images are converted to free surface slopes using a conversion table described in the previous section. The free surface elevation is then derived by integrating the slopes in the Fourier domain, as any function,  $f$ , can be represented by its Fourier transform

$$f(x, y) \Leftrightarrow F(k_x, k_y). \quad (8)$$

The derivatives of this function can be represented as a function of the Fourier transform of  $f$ ,

$$f_x(x, y) \Leftrightarrow ik_x F(k_x, k_y) = F_x(k_x, k_y) \quad (9)$$

$$f_y(x, y) \Leftrightarrow ik_y F(k_x, k_y) = F_y(k_x, k_y). \quad (10)$$

By rearranging and combining equations 2 and 3, the free surface elevation can be calculated as:

$$f(x, y) + C \Leftrightarrow F(k_x, k_y) = \frac{F_x(k_x, k_y) \cdot (-ik_x) + F_y(k_x, k_y) \cdot (-ik_y)}{k^2}, \quad (11)$$

where  $C$  is the constant of integration, and must be determined *a priori*. In this case,  $C$  represents the mean elevation of the free surface, and is set to zero.

## 2.2 Digital Particle Image Velocimetry (DPIV)

The DPIV processing technique used is a cross-correlation technique described by Willert & Gharib [14], incorporating the window-shifting technique developed by Westerweel et al. [12]. As DPIV has been well documented, only a brief description shall be discussed in this paper, and the reader is referred to Gharib & Dabiri [13] and its references for a full explanation of the cross-correlation DPIV.

The DPIV technique requires seeding the flow with optically reflective particles. Pulsed lasers (typically Nd:YAG lasers) are used to create a laser sheet to illuminate the cross-section of interest. A digital video camera captures sequential, singly-exposed images of the illuminated particle fields. For analysis, an interrogation window sub-samples identical portions of sequential image pairs. By calculation of a cross-correlation for the local interrogation window, a local velocity vector is obtained. Upon systematic scanning of the images with the interrogation window, a velocity vector field is thus obtained.

Since the particles move within the interrogation window, the number of particles common to both sequential images is less than the total particles within each of the windows, hence resulting in an uncertainty of ~3%, and ~6% in the velocity and vorticity measurements, respectively. By locally moving the interrogation window in the second of the sequential image pairs, using the DPIV results from the stationary interrogation window as a guide, it is possible to increase the number of the particles common to both sequential images. This procedure boosts the signal-to-noise ratio so that the velocity and vorticity measurement uncertainties are within 1% and 2%, respectively (Dabiri et al. [14]).

## 3 EXPERIMENTAL SETUP

To properly examine the concerns discussed above, an experiment was performed in a shear layer facility, with a test section 2 meters long, 1 meter wide, and 0.75 meters high (see figure 5). At rest, the water level is 56 cm. The shear layer is run such that the mean interface between the two free streams is perpendicular to the free surface, hence making this a vertical shear layer. The high speed side is run at 22.5 cm/s, and the low speed side is run at 10.5 cm/s. The Reynolds number, based on the average velocity of the mean streams and the vorticity thickness of the shear layer at the surface is 7425, and the Froude number, based on the velocity of the high-speed side and the water channel depth is 0.07.

The flow was interrogated using simultaneous measurements of both a DPIV system and a reflective Free Surface Gradient Detector (FSGD) system [5,8,10]. A horizontal 1 millimeter thick laser sheet was generated using a Nd:YAG laser, and placed just below the surface to allow for streamwise and spanwise velocity measurements, as well as the vertical vorticity component. Neutrally buoyant, silver-coated glass sphere particles with an average diameter of  $14 \pm 5 \mu\text{m}$  are used to seed the flow. A 1008\*1018 30 frames/second CCD camera was used to image a 22 by 22  $\text{cm}^2$  area. The time difference between pairs of images is 2 milliseconds. 32\*32 pixel interrogation windows were used with a 50% overlap in order to obtain vector maps of the imaged field of view. The FSGD system used a 640\*480 pixel 30 frame/second 3-CCD camera, which imaged the same area as the DPIV camera. While the DPIV system allows a 15 Hz data rate, the FSGD system allows for 30 Hz data rate. The two systems were synchronized by placing the FSGD exposure pulse between the two DPIV exposure pulses. The velocity uncertainties are within than 1%, since

a window shifting method was used [12]. Lastly, 2700 sequential data sets were used to obtain the statistical quantities shown below.

The FSGD technique is sensitive to the geometry of the set-up. Therefore, both the calibration and the experiment are done using the same set-up and within the same experimental facility. In order to be able to measure free surface deformations of large areas, it is necessary to use a large lens. Rather than using a large lens, a spherical mirror is used, which has the advantage of eliminating inaccuracies due to chromatic aberrations. The FSGD setup is shown in figure 6. It allows for ease of adjustment of distances between the mirror, color palette, and the light source, as well as the angle of this setup with respect to the free surface. The color palette used is shown in figure 4, and is 10.16 by 10.16 cm<sup>2</sup>. The mirror used is a 20.32 cm diameter front surface coated spherical mirror, with a 60.96 cm focal length. A linear Xenon strobe light is used for illumination, since Xenon provides a relatively uniform spectral response across the visible spectrum. The elevation range measured is  $\pm 1.2$  mm with a maximum measurement uncertainty of 6%.

Simultaneous acquisition of both free surface deformation and the near surface velocity field is ensured by synchronizing the horizontal and vertical drives of the DPIV camera with the FSGD camera. Figure 7 shows the pulse sequence of both the DPIV and FSGD cameras and their proper placements in relation to each other that ensures simultaneous data acquisition.

#### 4 DISCUSSION OF RESULTS

Two instantaneous results are shown in figures 10 and 11, which show a processed FSGD elevation field, and its near surface vorticity field at an instance in time, respectively. These figures show that the regions of high vorticity correspond to regions of free surface deformation. Most noticeable are the two regions of high vorticity, labeled *a* and *b* in figure 11, which are vortex tubes, which have connected to the free surface. These vortex tube connections are responsible for the free surface deformation “dimples”, labeled *a* and *b*, as shown in figure 10.

The attached video shows the instantaneous correlation between the free surface deformation and the near surface vorticity in time. The top left image is the instantaneous free surface deformation, the bottom left is the instantaneous vorticity field, and the top right and bottom right images are the instantaneous correlations between the two. The dark dimples seen in the instantaneous deformation field are the local deformations due to the reconnected vortex tubes. The vorticity associated with these tubes can be seen in the vorticity field and are represented by the dark spots. In watching the video, it is clear that the free surface dimples seen in the deformation field correlate very well with the regions of high vorticity seen in the vorticity field.

Though the instantaneous correlations discussed above are impressive, it is more appropriate to average this correlation through time. Figure 17 shows the normalized correlation between the free surface deformation and the near surface vertical vorticity component. For this plot, the axes are rearranged so that the high speed side is on the right, while the low speed side is on the left. Furthermore, the dividing streamline is set as the origin of the spanwise direction (shown on the x-axis of the plots). The spanwise direction is then normalized by the local vorticity thickness, and the correlations are normalized by the vorticity thickness, the free streams' velocity and height difference. Six downstream spanwise profiles are plotted within the range  $x \hat{I}$  [26, 46] cm. It is seen that the correlations increase with downstream distance, and are maximum on the shear layer centerline. Furthermore, it was found that the correlation coefficient is 0.4, indicating that the correlation seen is in fact quite strong, indicating that the free surface deformation correlates very well with the near surface vorticity. In fact, this confirms the work of Dommermuth et al. [1], who showed and explained that for low Froude numbers, ‘the surface elevation is hydrostatically balanced by the vortically-induced pressure’, indicating it is the vorticity that is directly responsible for the free surface deformations.

The pressure spectra of the shear layer at various spanwise locations across the shear layer is shown at a downstream distance of 35 cm in figure 11. According to George et al. [3], in the inertial range, the slope should be  $-11/3$ . For the present result, it is seen that for spanwise locations of  $x/d_w \leq |1.5|$ , the spectra show a logarithmic distribution with a  $-10/3$  slope. Outside of this region, which corresponds to the freestream, the spectra does not display a logarithmic

distribution, showing that these regions of the flow are turbulent-free. As the effects of the 2<sup>nd</sup> moment turbulence-mean shear interaction cannot be separated from the 3<sup>rd</sup> moment turbulent-mean-shear interaction and the turbulence-turbulence interaction, the present measurement represents a combination of all three of these terms. However, the dominant effect of the 2<sup>nd</sup> moment turbulence-mean shear interaction can be seen as the present measured slope of  $-10/3$  is very close to the theoretically derived value of  $-11/3$ .

## 5 CONCLUSION

In conclusion, the simultaneous DPIV and FSGD have been successfully used to map the vertical shear layer interaction with a free surface in a low Froude number environment. The correlation between the vorticity and the pressure shows that the correlation is in fact strong, confirming the findings of Dommermuth [1]. The results also show that the pressure spectra measured through the surface deformation measurements show a  $-10/3$  slope within the shear layer, thus confirming the results of Beuther et al. and George et al. In the future plan to combine the FSGD method with stereo DPIV in order to allow for acquisition of all components of velocity, as well as deformation. This will then allow us ascertain the role of the turbulent kinetic energy in near surface flows.

## 6 ACKNOWLEDGEMENT

The authors gratefully acknowledge the support of the Office of Naval Research under the research grant number N00014-97-1-0303.

## 7 REFERENCES

- [1] Dommermuth, D.G.; Novikov, E. & Mui R., 1994 The interaction of surface waves with turbulence *Free-Surface Turbulence ASME Meeting*, FED-Vol. 181, 123-140.
- [2] Beuther, P.D., George, W.K., & Arndt, R.E.A., 1977, Modeling of Pressure Spectra in a Turbulent Shear Flow, *Acoustical Society of America Meeting*, State College, Pa. June 6-10.
- [3] George, W. K., Beuther, P.D. & Arndt, R.E.A., 1984, Pressure spectra in turbulent free shear flows, *J.F.M.*, 148, 155-191.
- [4] Cox, C.S. 1958; Measurement of slopes of high-frequency wind waves, *J. Mar. Res.*, 16, 199.
- [5] Zhang, X.; & Cox, C.S. 1994; Measuring the Two-Dimensional structure of a wavy water surface optically: a surface gradient detector, *Exp. Fluids*, 17, 225-237
- [6] Jahne, Bernd, *Image Processing for Scientific Applications*, CRC Press, New York, 1997
- [7] Balschbach, G., Klinke, G., and Jähne, B. 1998 Multichannel shape from shading techniques for moving specular surfaces, *Computer Vision (ECCV '98)*, Proc. Vol. II, H. Burkhardt and B. Neumann (eds.), *Lecture Notes in Computer Science 1407*, Springer-Verlag, Berlin, pp. 170-184.
- [8] The DPIV processing technique used is a cross-correlation technique described by Willert & Gharib [14], incorporating the window-shifting technique developed by Westerweel et al. [12]. As DPIV has been well documented, only a brief description shall be discussed in this paper, and the reader is referred to Gharib & Dabiri [13] and its references for a full explanation of the cross-correlation DPIV.
- [9] Zhang, X.; Dabiri, D. & Gharib, M. 1996; Optical mapping of fluid density interfaces: Concepts and implementations, *Rev. of Sci. Inst.*, 67, 5, 1858-1868
- [10] Dabiri, D.; Zhang, X. & Gharib, M. 1997; Quantitative Visualization of Three-Dimensional Free Surface Slopes & Elevations, *Atlas of Visualization*, Boca Raton, CRC Press LLC, Editor: Yasuki Nakayama.
- [11] Willert, C. & Gharib, M. 1991; Digital particle image velocimetry. *Exp. Fluids* 10:181-193.
- [12] Westerweel, J.; Dabiri, D. & Gharib, M. 1997; The effect of a discrete window offset on the accuracy of cross-correlation analysis of digital PIV recordings. *Exp. Fluids*, 23:20-28
- [13] Gharib, M. & Dabiri, D. 1999; *Digital Particle Image Velocimetry*, Flow Visualization: Techniques and Examples, Ed. A.J Smits and T.T. Lim, Imperial College Press, 123-148.
- [14] Dabiri, D.; Westerweel, J.; Jeon, D.; & Shan, J. 1995; On the effects of window shifting and image windowing for improved accuracy of velocity measurements for DPIV, *American Physical Society, 48<sup>th</sup> Annual Meeting of the Division of Fluid Dynamics*, November 19-21, Irvine, California.

INTERACTION OF A SHEAR LAYER WITH A FREE SURFACE

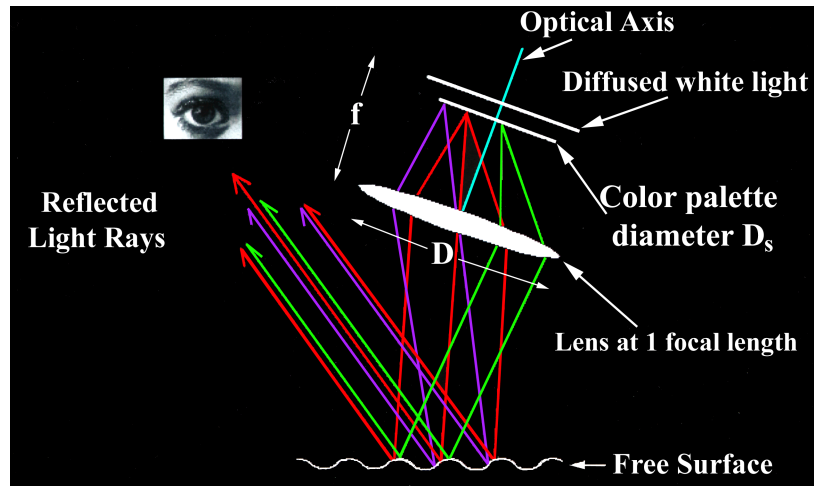


Figure 1: Reflective mode setup of the free surface gradient detector.

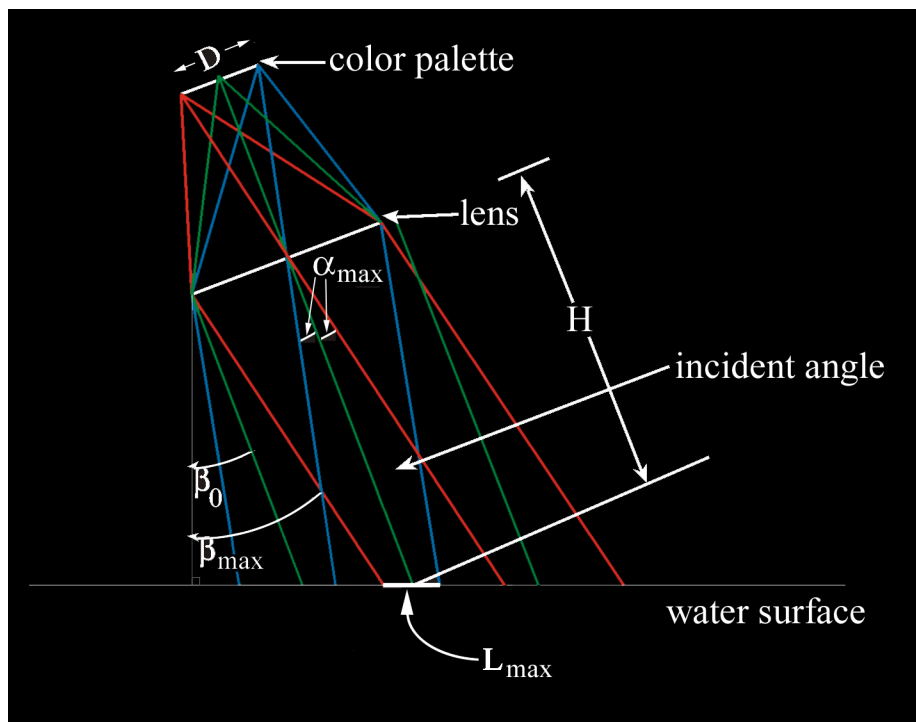


Figure 2: Optical setup and ray tracing showing the measurable area of the free surface.

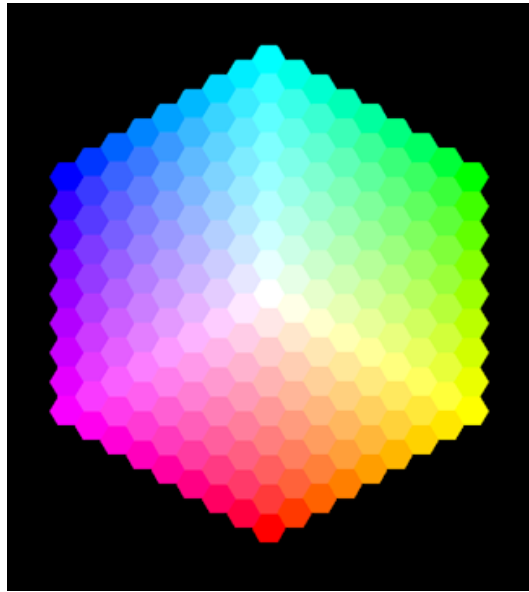


Figure 3: Discrete color palette.

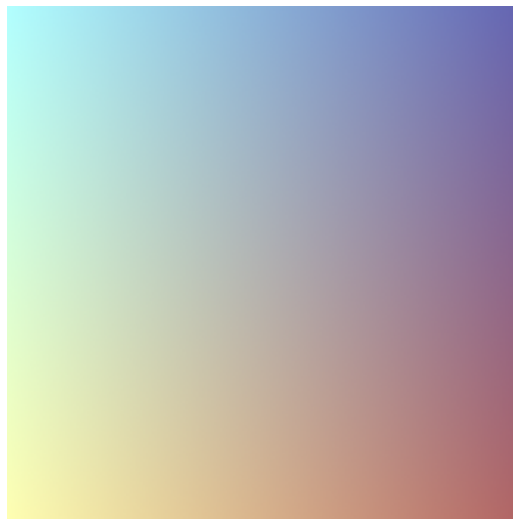
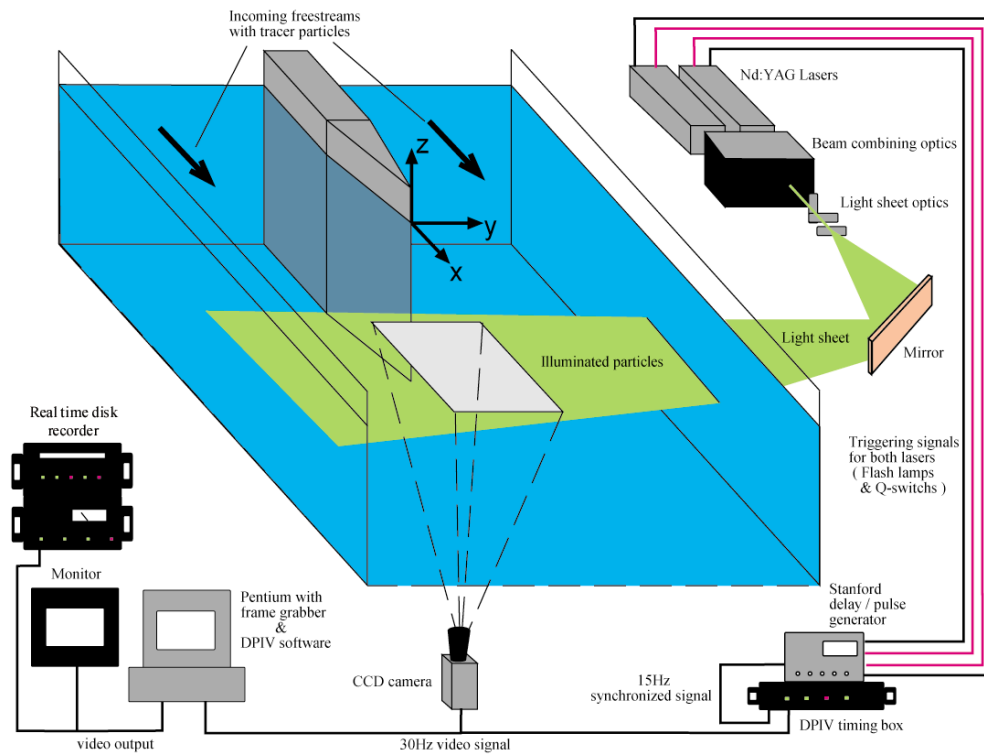
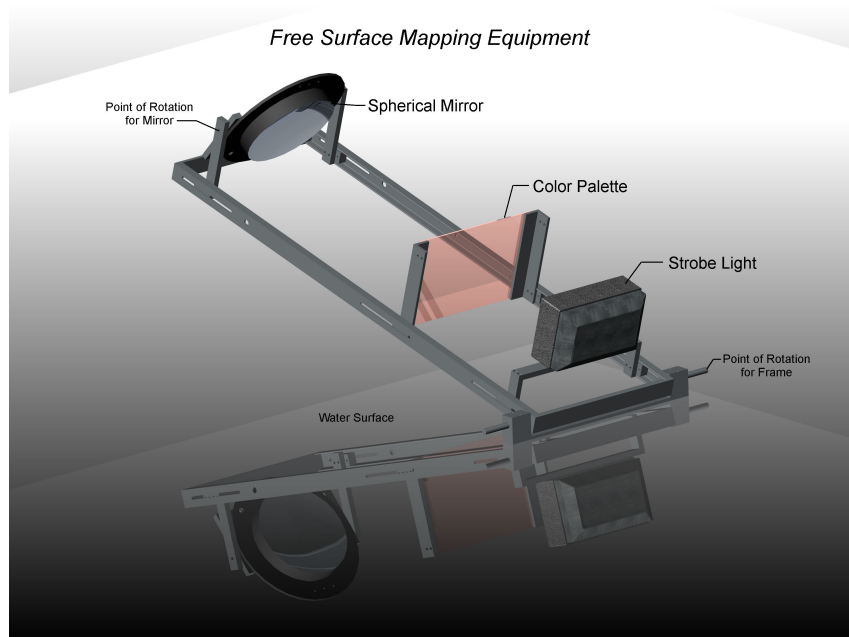


Figure 4: Continuously varying color map.

## INTERACTION OF A SHEAR LAYER WITH A FREE SURFACE



**Figure 5: Free shear tunnel facility with DPIV experimental setup.**



**Figure 6: Free surface gradient detector setup.**

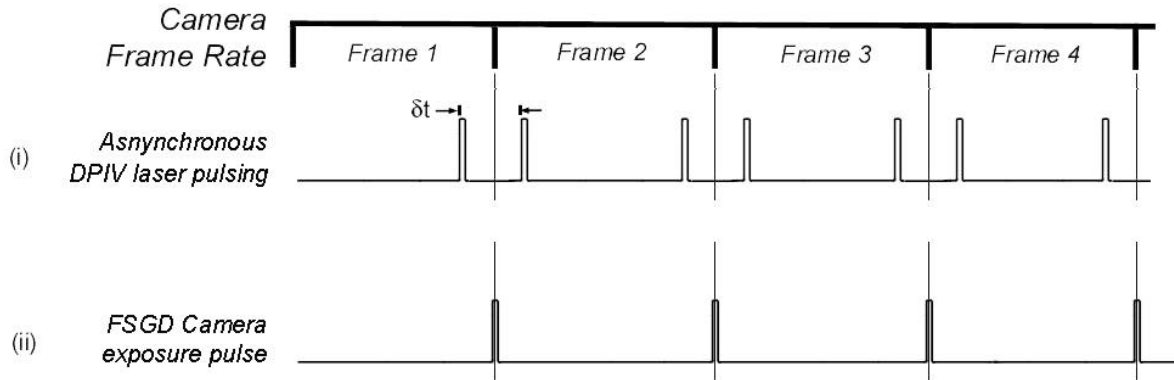


Figure 7: Exposure sequence and synchronization for the DPIV and FSGD cameras.

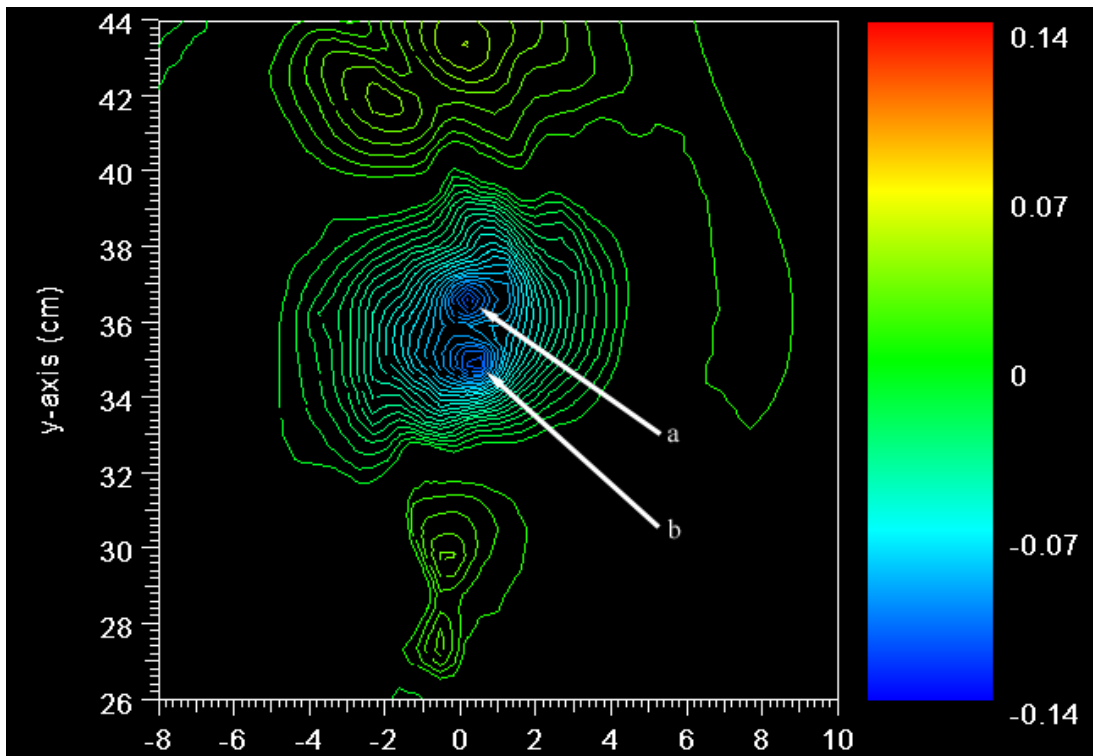


Figure 8: An instantaneous free surface elevation plot. Contours are 0.014 cm per level. Axes are in cm.

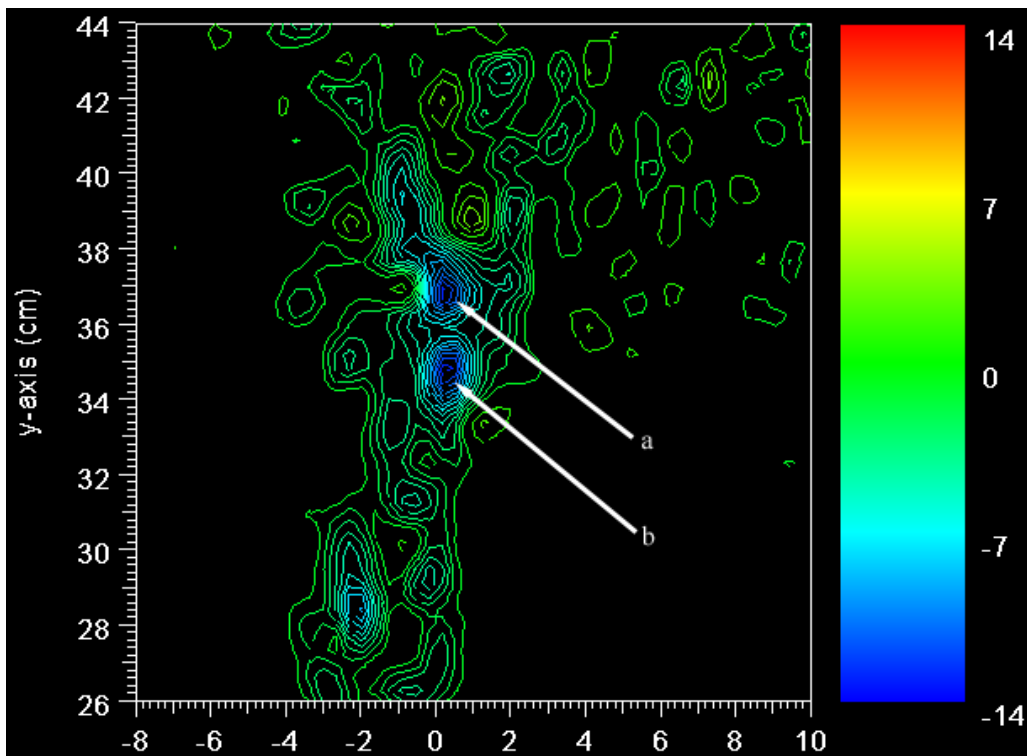


Figure 9: Near surface instantaneous vorticity plot. Axes are in cm.

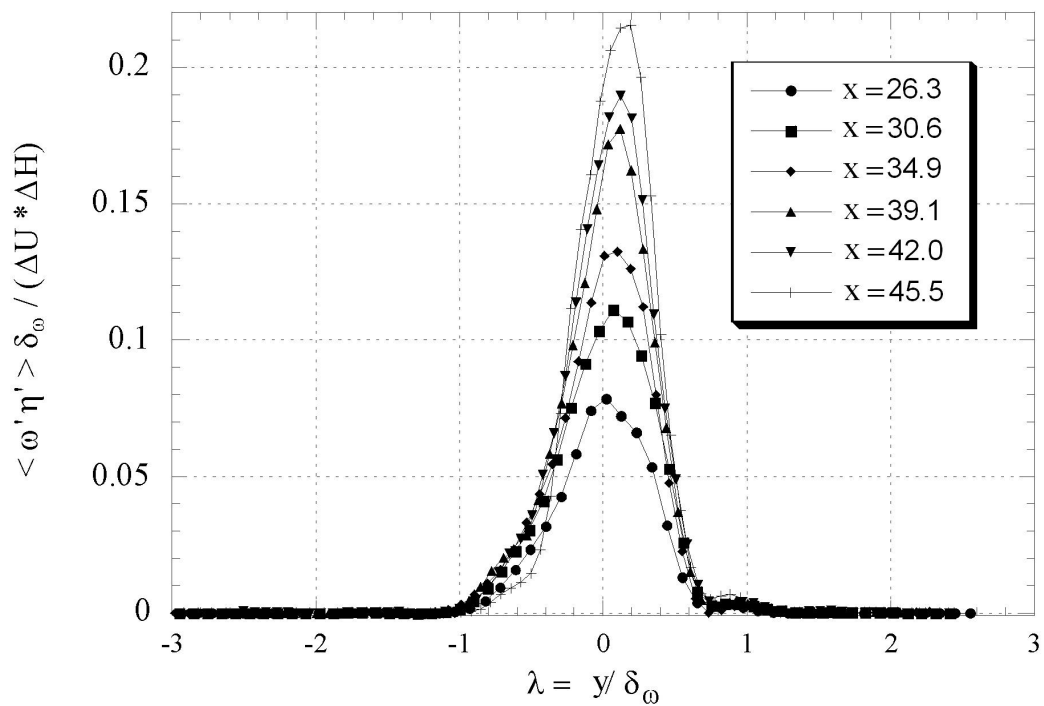


Figure 10: Mean normalized vertical-vorticity/elevation correlation profiles at various downstream locations

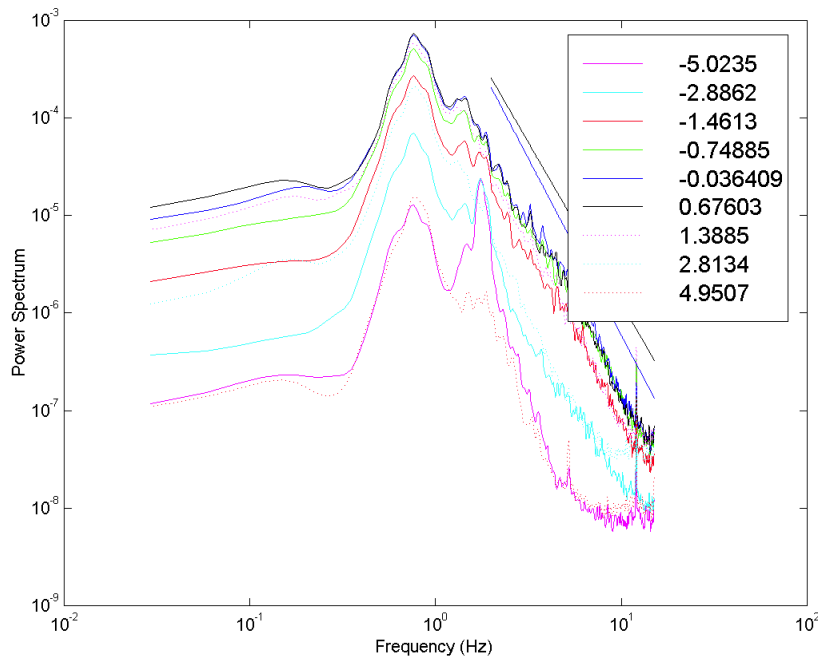


Figure 11: Spanwise pressure spectra for various  $y/dw$  at  $x = 35$  cm